Astronomy & Astrophysics manuscript no. 15574
October 11, 2010

An optical spectroscopic survey of the 3CR sample of radio galaxies with $z < 0.3$.

III. Completing the sample⋆

Sara Buttiglione[1,2], Alessandro Capetti[3], Annalisa Celotti[2], David J. Axon[4,5], Marco Chiaberge[6,7], F. Duccio Macchetto[6], and William B. Sparks[6]

[1] INAF, Osservatorio Astronomico di Padova, Vicolo dell'Osservatorio 5, I-35122 Padova, Italy e-mail: sara.buttiglione@oapd.inaf.it
[2] SISSA-ISAS, Via Beirut 2-4, I-34014 Trieste, Italy
[3] INAF - Osservatorio Astronomico di Torino, Strada Osservatorio 20, I-10025 Pino Torinese, Italy
[4] School of Mathematical and Physical Sciences, University of Sussex, Falmer, Brighton BN1 9RH, UK
[5] Department of Physics, Rochester Institute of Technology, 85 Lomb Memorial Drive, Rochester, NY 14623, USA
[6] Space Telescope Science Institute, 3700 San Martin Drive, Baltimore, MD 21218, U.S.A.
[7] INAF-Istituto di Radio Astronomia, via P. Gobetti 101, I-40129 Bologna, Italy

ABSTRACT

We present optical nuclear spectra for nine 3CR radio sources obtained with the Telescopio Nazionale Galileo, that complete our spectroscopic observations of the sample up to redshifts < 0.3. We measure emission line luminosities and ratios, and derive a spectroscopic classification for these sources.

Key words. galaxies: active, galaxies: jets, galaxies: elliptical and lenticular, cD, galaxies: nuclei

1. Introduction

The 3CR catalog of radio sources represents a particularly well suited sample for a study of the physics of radio-loud AGN. Its selection criteria are unbiased with respect to optical properties and orientation, and it spans a relatively wide range in redshift and radio power. A vast suite of observations is already available for this sample, from multi-band HST imaging, to observations with Chandra, Spitzer and the VLA.

Quite surprisingly, however, the available optical spectroscopic data for the 3CR sample were sparse and incomplete. To fill this gap, we carried out a homogeneous and complete survey of optical spectroscopy, targeting the subsample of 113 3CR radio sources with z<0.3, for which we can obtain uniform uninterrupted coverage of the key spectroscopic optical diagnostics. The observed sources include a significant number of powerful classical FR II RG, as well as the more common (at low redshift) FR Is (Fanaroff & Riley 1974), spanning four orders of magnitude in radio luminosity, thus providing a broad representation of the spectroscopic properties of radio-loud AGN. The data were presented in Buttiglione et al. (2009) (hereafter Paper I) and discussed in Buttiglione et al. (2010) (hereafter Paper II).

However, nine sources of our sample (namely 3C 020, 3C 063, 3C 132, 3C 288, 3C 346, 3C 349, 3C 403.1, 3C 410, 3C 458) could not be observed due to scheduling problems and time constraints. Furthermore, the SDSS spectrum of 3C 270 presented in Paper I could not be used for its spectroscopic characterization, since the fiber was not positioned on the galaxy's nucleus (Christian Leipski, private communication). In order to reach completeness of the spectroscopic survey we present the results of new TNG observations of nine missing sources, while we complemented our data with those obtained for 3C 270 by Ho et al. (1997).

The paper is organized as follows: in Sect. 2 we present the observational procedure and the data reduction, leading to the measurements of the emission line fluxes (Sect. 3). In Sect. 4 we derive a spectroscopic classification for these sources, updating the results derived in Paper II. A brief summary is given in Sect. 5.

Throughout, we have used $H_o = 71$ km s^{-1} Mpc^{-1}, $\Omega_\Lambda = 0.73$ and $\Omega_m = 0.27$.

2. Observations and data reduction

The optical spectra of the nine missing 3CR sources were taken with the Telescopio Nazionale Galileo (TNG), a 3.58 m telescope located on the Roque de los Muchachos in La Palma Canary Island (Spain). The observations were made with the DOLORES (Device Optimized for the LOw RESolution) spectrograph. The detector used is a 2100x2100 pixels back-illuminated E2V4240, with a pixel size of $0\farcs252$. The observations were carried out in service mode between September 2008 and July 2009. The chosen

Send offprint requests to: S. Buttiglione

⋆ Based on observations made with the Italian Telescopio Nazionale Galileo operated on the island of La Palma by the Centro Galileo Galilei of INAF (Istituto Nazionale di Astrofisica) at the Spanish Observatorio del Roque del los Muchachos of the Instituto de Astrofsica de Canarias.

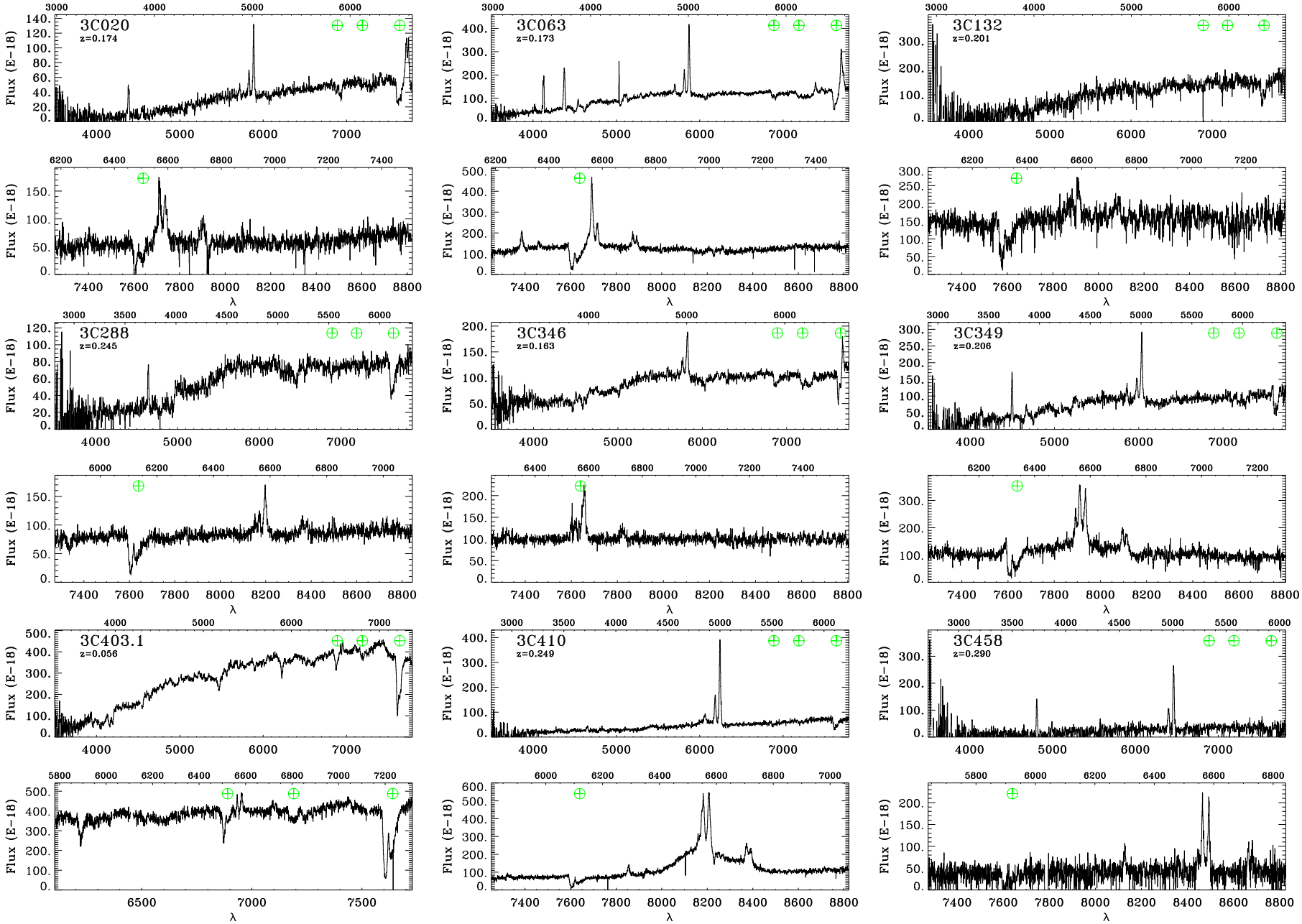

Fig. 1. For each source the low (upper panels) and high resolution (bottom panels) spectra are shown. The fluxes are in units of erg cm^{-2} s^{-1} Å^{-1} while the wavelengths are in Å. The lower axes of the spectra show the observed wavelengths while the upper axes show the rest frame wavelengths. The three main telluric absorption bands are indicated with circled crosses.

long-slit width is 2″ and it was aligned along the parallactic angle in order to minimize light losses due to atmospheric dispersion.

For each target we took one (or two) low resolution spectrum with the LR-B grism (∼3500-7700 Å) with a resolution of ∼20 Å and two high resolution spectra with the VHR-R (6100-7700 Å) or VHR-I (7250-8800 Å) grisms, depending on redshift, with a resolution of ∼5 Å. The exposure times increase with redshift, in order to compensate for the galaxies' dimming. Exposures longer than 750 s were divided into two sub-exposures of 500 sec, obtained moving the target along the slit. The high resolution spectra have an exposure time twice the low resolution ones. The combination of the LR-B and VHR ranges of wavelengths enables us to cover the most prominent emission lines of the optical spectrum and in particular the key diagnostic lines Hβ, [O III]$\lambda\lambda$4959,5007, [O I]$\lambda\lambda$6300,64, Hα, [N II]$\lambda\lambda$6548,84, [S II]$\lambda\lambda$6716,31. The high resolution spectra are a sort of *zoom* on the Hα region with the aim of resolving the Hα from the [N II] doublet, as well as the two lines of the [S II] doublet. Table 1 provides the journal of observations and the main information on the sources.

The data analysis was performed as describer in Paper I, which should be refer to for further details. Summarizing the spectra were bias subtracted and flat fielded. When the spectra were split into two sub-exposures, they were subtracted to remove the sky background. The residual background was subtracted measuring the average on each pixel along the dispersion direction in spatial regions immediately surrounding the source spectrum. The data were then wavelength calibrated and corrected for optical distortions. Finally the spectra were extracted and summed over a region of 2″ along the spatial direction and flux calibrated using spectrophotometric standard stars, observed immediately after each target.

The telluric absorption bands were usually left uncorrected except in the few cases in which an emission line of interest fell into these bands. In these cases we corrected the atmospheric absorptions using the associated standard stars as templates.

Fig. 1 shows, for all the observed targets, the low resolution spectrum (upper image) and the high resolution one (bottom image). The calibrated spectra are in units of 10^{-18} erg cm^{-2} s^{-1} Å^{-1}. The wavelengths (in Å units) are in the observer frame in the axes below the images while they are in the source frame in the axes above them.

3. Data analysis

We corrected the spectra for reddening due to the Galaxy (Burstein & Heiles 1982, 1984) using the extinction law of Cardelli et al. (1989). The galactic extinction used for each object was taken from the NASA Extragalactic Database (NED) database and is listed in Table 2. We also transform the spectra into rest frame wavelengths using the value of redshift from NED.

The contribution of stars to our spectra was subtracted using the best fit single stellar population (SSP) model taken from the Bruzual & Charlot (2003) library out of a grid of 33 single stellar population models, with a Salpeter Initial Mass Function, formed in an instantaneous burst. We excluded from the fit the spectral regions corresponding to emission lines, as well as other regions affected by telluric absorption, cosmic rays or other impurities. In 3C 410 the continuum is essentially featureless and it is likely to be dominated by non-stellar emission, a characteristic already seen in several 3CR objects. No starlight subtraction was performed for this object.

By using the *specfit* package in IRAF, we then measured line intensities fitting Gaussian profiles to Hβ, [O III]$\lambda\lambda$4959,5007, [O I]$\lambda\lambda$6300,64, Hα, [N II]$\lambda\lambda$6548,84, and [S II]$\lambda\lambda$6716,31. Some constraints were adopted to reduce the number of free parameters: we required the widths and the velocity to be the same for all the lines. The integrated fluxes of each line were free to vary except for those with known ratios from atomic physics: i.e. the [O I]$\lambda\lambda$6300,64, [O III]$\lambda\lambda$4959,5007 and [N II]$\lambda\lambda$6548,84 doublets. Prominent broad Hα and Hβ lines are visible in the spectrum of 3C 410. We then fit the line emission including a broad component. This is well reproduced by a gaussian profile, when allowing a small line asymmetry.

Table 2 summarizes the intensities of the main emission lines (de-reddened for Galactic absorption) relative to the intensity of the narrow component of Hα, for which we give flux and luminosity. To each line we associated its relative error, as a percentage. We placed upper limits at a 3σ level to the undetected, but diagnostically important, emission lines by measuring the noise level in the regions surrounding the expected positions of the lines, and adopting as line width the instrumental resolution. In the case of 3C 346 the telluric correction is not sufficiently accurate to recover the flux of its Hα line, that falls in a deep transmission through of a telluric band. For 3C 410 we also give the flux of its broad Hα line.

4. Results

The data quality of the nine spectra considered here is such that we could measure all diagnostic lines with only three exceptions: [O I] in 3C 132, Hα in 3C 346 due to a telluric band, and Hβ in 3C 458. We complemented our observations with the data for 3C 270 from Ho et al. (1997) that were obtained using a similar extraction aperture and spectral resolution. Following Paper II we used the Excitation Index (E.I.), defined as

E.I. = Log [O III]/Hβ - 1/3 (Log [N II]/Hα+ Log [S II]/Hα+ Log [O I]/Hα)

to derive an optical spectroscopic classification of the eight sources where all six diagnostic lines could be measured. Defining as LEG the sources with E.I. $\lesssim 0.95$, four of them are LEG and four are HEG (see Table 3). For 3C 132 we lack the measurement of its [O I] line; however, this source is located well within the region of LEG in the diagnostic diagrams, see Fig. 2, where it is represented by the filled triangle. Conversely, 3C 346, without a Hα flux estimate, could not be classified based on the emission line ratios; similarly we cannot derive a classification from the diagrams comparing lines and radio luminosity since its location in Fig. 3 (the filled triangle in the left panel) is between the relations defined by LEG and HEG. Instead 3C 458 can be defined as HEG, although the Hβ line cannot be measured, from the lower limit (E.I. > 1.03) derived for this source.

Including 3C 410 there are now 19 3CR radio-galaxies with broad lines. In agreement with our previous findings, also 3C 410 is a HEG from the point of view of its narrow line ratios. The four newly discovered HEG are of high total

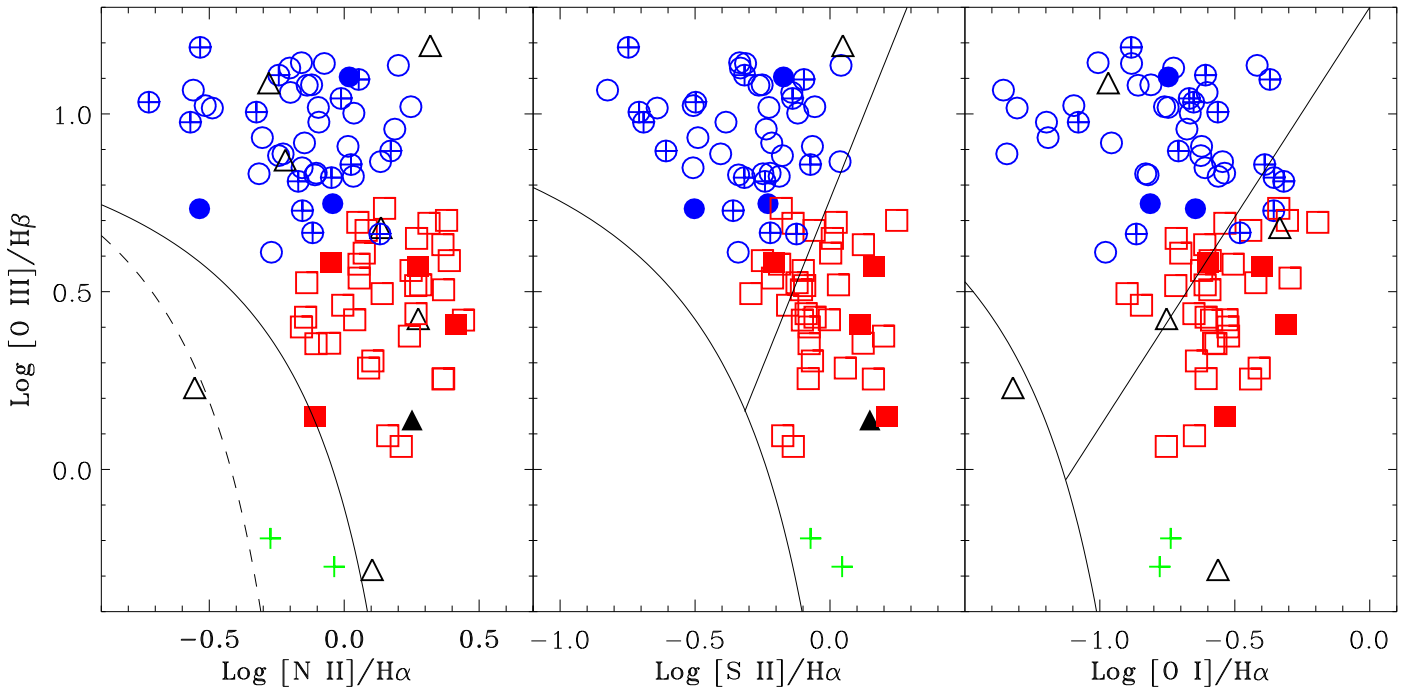

Fig. 2. Diagnostic diagrams for 3CR sources after the classification into HEG (blue circles) and LEG (red squares) made using the Excitation Index. Crossed circles are broad line galaxies, green crosses are extremely low [O III]/Hβ sources. Black triangles are sources for which the E.I. cannot be estimated, as they lack the measurement of one or two diagnostic lines. The filled symbols are derived from the new data presented in this paper.

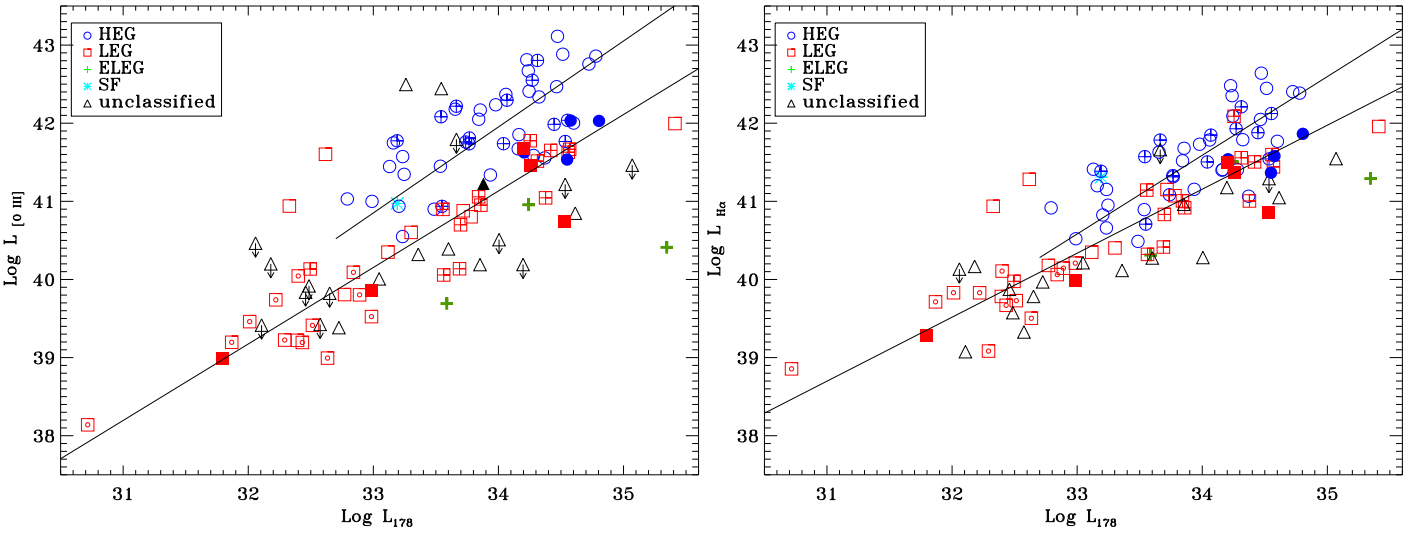

Fig. 3. [O III] and Hα luminosity [erg s^{-1}] (left and right panel, respectively) as a function of radio luminosity at 178 MHz [erg s^{-1} Hz^{-1}]. Blue circles are HEG (crossed circles are BLO), red squares are LEG, green pluses are ELEG, the cyan asterisk is the star forming galaxy, while the black triangles are spectroscopically unclassified galaxies. The two solid lines represent the best linear fit obtained for the HEG and LEG sub-populations separately. When possible, we further mark the LEG according to their FR type: crossed squares are FR II/LEG and dotted squares are FR I/LEG. The filled symbols are derived from the new data presented in this paper.

Table 1. Log of the observations.

Name	Coordinates J2000		z	Obs. Date	Low Res.		High Res.			Notes
	α	δ			n	T_{exp}	HR	n	T_{exp}	
3C 020	00 43 09.27	+52 03 36.66	0.174	22Sep08	1	750	HRI	2	750	
3C 063	02 20 53.82	–01 57 54.08	0.175	23Sep08	1	750	HRI	2	750	
3C 132	04 56 43.40	+22 49 21.62	0.214	23Oct08	2	500	HRI	2	1000	
3C 288	13 38 50.00	+38 51 10.70	0.246	18Jan09	2	500	HRI	2	1000	
3C 346	16 43 48.69	+17 15 48.09	0.161	01Sep08	1	750	HRI	2	750	i
3C 349	16 59 28.84	+47 02 56.80	0.205	30Aug08	2	500	HRI	2	1000	
3C 403.1	19 52 30.58	–01 17 19.68	0.055	22Sep08	1	500	HRR	2	500	
3C 410	20 20 06.56	+29 42 14.20	0.249	23Sep08	2	500	HRI	2	1000	f,g
3C 458	23 12 54.40	+05 16 46.00	0.289	29Lug09	2	500	HRI	2	1000	

Column description: (1) 3C name of the source; (2) and (3) J2000 coordinates (right ascension and declination); (4) redshift; (5) UT night of observation; (6) number of low resolution spectra; (7) exposure time for each low resolution spectrum; (8) high resolution grism used; (9) number of high resolution spectra; (10) exposure time for each high resolution spectrum. (11): (f) broad components; (g) no starlight subtraction; (i) telluric correction.

Table 2. Emission line measurements.

Name	Redshift	E(B-V)	L(Hα)	F(Hα)	Hβ	[O III]λ5007	[O I]λ6300	[N II]λ6584	[S II]λ6716	[S II]λ6731	F(Hα) broad
3C 020	0.175	0.407	41.37	-14.55 (4)	0.26 (10)	1.48 (2)	0.15 (17)	0.91 (3)	0.33 (1)	0.26 (5)	
3C 063	0.173	0.027	41.54	-14.38 (5)	0.23 (4)	1.22 (1)	0.23 (3)	0.29 (2)	0.18 (4)	0.13 (5)	
3C 132	0.201	0.482	41.37	-14.75 (1)	0.90 (5)	1.24 (2)	<0.20	1.78 (1)	0.67 (2)	0.73 (2)	
3C 288	0.245	0.007	40.86	-15.40 (6)	0.58 (17)	0.62 (16)	0.40 (13)	1.87 (3)	0.85 (7)	0.60 (9)	
3C 346	0.163	0.067	41.24[a]	-14.62[a] (1)	0.20[a] (10)	1.00[a] (2)	0.14[a] (14)	0.84[a] (4)	0.13[a] (11)	0.13[a] (11)	
3C 349	0.206	0.031	41.50	-14.58 (2)	0.40 (6)	1.54 (2)	0.25 (13)	0.90 (2)	0.34 (5)	0.28 (8)	
3C 403.1	0.056	0.234	39.99	-14.87 (15)	0.53 (13)	0.75 (7)	0.29 (17)	0.78 (6)	0.90 (3)	0.72 (11)	
3C 410	0.249	0.050	41.86	-14.40 (8)	0.12 (13)	1.46 (1)	0.18 (9)	1.04 (1)	0.37 (3)	0.30 (3)	-13.47 (1)
3C 458.0	0.289	0.082	41.58	-14.84 (4)	<0.45	2.85 (3)	0.33 (14)	0.91 (3)	0.36 (4)	0.31 (8)	
3C 270	0.007	0.018	39.26	-13.80	0.20	0.51	0.49	2.60	0.72	0.57	

Column description: (1) source name; (2) redshift; (3) Galactic absorption; (4) logarithm of the luminosity of the Hα narrow line, in erg s^{-1}; (5) logarithm of the Hα flux in erg cm^{-2} s^{-1}; (6 through 11) de-reddened flux ratios of the key diagnostic lines with respect to Hα. The values in parentheses report the errors (in percentage) of each line; (12) logarithm of the flux of the Hα broad component, when visible. Notes: (a) for 3C 346 no measurement of Hα is possible and we give instead the [O III] luminosity, referring the flux ratios to this line. Data for 3C 270 are taken from Ho et al. (1997) and corrected for Galactic reddening.

radio-power, Log $L_{178} > 32.8$ [$\mathrm{erg\,s^{-1}\,Hz^{-1}}$], and with a FR II morphology, a result that applies to all object of this spectroscopic sub-class.

The number of LEG with high radio luminosity, Log $L_{178} > 34$ [$\mathrm{erg\,s^{-1}\,Hz^{-1}}$], and a FR II morphology is significantly increased by the new observations (with the additions of 3C 132, 3C 288, and 3C 349), from six to nine objects, confirming the relevance of this subclass.

In Paper II we derived the best fit correlation for the link between line luminosity with radio power, considering separately the sub-populations of HEG and LEG. Including the new sources we find:

Log $L_{[\mathrm{O\ III}]} = 1.10$ Log $L_{178} + 4.54$ (for HEG) and
Log $L_{[\mathrm{O\ III}]} = 0.98$ Log $L_{178} + 7.86$ (for LEG).
Considering instead the Hα line we have
Log $L_{\mathrm{H}\alpha} = 1.01$ Log $L_{178} + 7.35$ (for HEG) and
Log $L_{\mathrm{H}\alpha} = 0.82$ Log $L_{178} + 13.31$ (for LEG).

The slopes of the correlations are only marginally reduced with respect to the values reported in Paper I, by 0.05 and 0.01 for HEG and LEG respectively, for both lines. The errors in the slopes are also marginally reduced to 0.10 (0.09) for the relation between $L_{[\mathrm{O\ III}]}$ and Log L_{178} for HEG (LEG).

5. Summary

We presented optical spectroscopic data of nine 3CR radio sources, needed to complete our survey of this catalogue with redshift < 0.3, and measured emission lines luminosities and ratios. These data enabled us to derive an optical spectroscopic classification for all but one galaxy. The relationships between spectroscopic and radio properties found from our previous works, are confirmed by the analysis of the now complete sample.

Acknowledgements. SB and ACe acknowledge the Italian MIUR for financial support. ACa acknowledges COFIN-INAF-2006 grant financial support. This research has made use of the NASA/IPAC Extragalactic Database (NED) which is operated by the Jet Propulsion Laboratory. California institute of Technology, under contract with the National Aeronautics and Space Administration. This research has made use of NASA's Astrophysics Data System (ADS).

References

Baldi, R. D. & Capetti, A. 2009, A&A, 508, 603
Bruzual, G. & Charlot, S. 2003, MNRAS, 344, 1000
Burstein, D. & Heiles, C. 1982, AJ, 87, 1165
Burstein, D. & Heiles, C. 1984, ApJS, 54, 33
Buttiglione, S., Capetti, A., Celotti, A., et al. 2009, A&A, 495, 1033 (Paper I)
Buttiglione, S., Capetti, A., Celotti, A., et al. 2010, A&A, 509, A6 (Paper II)
Cardelli, J. A., Clayton, G. C., & Mathis, J. S. 1989, ApJ, 345, 245
Donzelli, C. J., Chiaberge, M., Macchetto, F. D., et al. 2007, ApJ, 667, 780
Fanaroff, B. L. & Riley, J. M. 1974, MNRAS, 167, 31P
Ho, L. C., Filippenko, A. V., & Sargent, W. L. W. 1997, ApJS, 112, 315
Skrutskie, M. F., Cutri, R. M., Stiening, R., et al. 2006, AJ, 131, 1163
Spinrad, H., Marr, J., Aguilar, L., & Djorgovski, S. 1985, PASP, 97, 932

Table 3. Multiwavelength data and spectroscopic classification

Name	redshift	Emission lines		Radio emission		Host magnitude	Classification		
		Hα	[O III]	L_{178}	P_{core}	M_H	FR	spec	Method
3C 020	0.174	41.37	41.54	34.55	30.44	-24.64*	2	HEG	E.I.
3C 063	0.175	41.54	41.63	34.21	31.12	–		HEG	E.I.
3C 132	0.214	41.37	41.46	34.25	31.58	-26.00	2	LEG	D.D.
3C 270	0.007	39.26	38.96	31.79	29.57	-25.01	1	LEG	E.I.
3C 288	0.246	40.86	40.65	34.53	31.73	-26.10*	2	LEG	E.I.
3C 346	0.161	–	41.24	33.88	32.18	-25.84	2	–	
3C 349	0.205	41.50	41.69	34.20	31.35	-24.82*	2	LEG	E.I.
3C 403.1	0.055	39.99	39.86	32.98	–	-24.36		LEG	E.I.
3C 410	0.248	41.86	42.02	34.80	33.43	–	2	BLO	E.I.
3C 458	0.289	41.58	42.03	34.58	30.88	–	2	HEG	E.I.

Column description: (1) 3CR name; (2) redshift from Spinrad et al. (1985); (3) and (4) logarithm of Hα and [O III]λ5007 luminosities [erg s^{-1}]; (5) radio luminosity at 178 MHz [erg s^{-1} Hz^{-1}] from Spinrad et al. (1985); (6) radio core power at 5 GHz [erg s^{-1} Hz^{-1}] from Baldi & Capetti (2009); (7) host H magnitude from 2MASS (Skrutskie et al. 2006) (or from HST (Donzelli et al. 2007) for the objects marked with a *); (8): morphological FR type; (9) spectroscopic classification into High Excitation Galaxy (HEG); Low Excitation Galaxy (LEG); Broad Line Object (BLO); (–) unclassified. Column (10) classification method: E.I. - excitation index; D.D. - diagnostic diagrams.

Appendix A: Additional material

In the following two tables we provide the data for the whole 3CR sub-sample of radio galaxies with $z < 0.3$ combining the results presented here with those of Paper I and Paper II. This is additional material with respect to the article published in Astronomy & Astrophysics.

Table A.1. Emission line measurements.

Name	Redshift	E(B-V)	L(Hα)	F(Hα)	Hβ	[O III]λ5007	[O I]λ6364	[N II]λ6584	[S II]λ6716	[S II]λ6731	F(Hα) broad
3C 015.0	0.073	0.022	40.40	-14.70 (2)	0.32 (20)	1.58 (4)	0.29 (8)	2.06 (1)	0.32 (8)	0.41 (8)	
3C 017.0	0.220	0.023	41.88	-14.27 (1)	0.24 (8)	1.28 (1)	0.44 (1)	0.70 (1)	0.23 (1)	0.21 (2)	-13.87
3C 018.0	0.188	0.158	41.93	-14.06 (1)	0.33 (1)	4.17 (1)	0.43 (3)	1.13 (1)	0.38 (2)	0.42 (1)	-13.03
3C 020.0	0.175	0.407	41.37	-14.55 (4)	0.26 (10)	1.48 (2)	0.15 (17)	0.91 (3)	0.33 (1)	0.26 (5)	
3C 028.0	0.195	0.058	41.51	-14.52 (2)	0.53 (15)	0.28 (20)	0.17 (10)	0.92 (3)	0.55 (10)	–	
3C 029.0	0.045	0.036	40.06	-14.60 (6)	0.24 (25)	1.07 (2)	0.19 (16)	1.85 (1)	0.50 (6)	0.52 (4)	
3C 031.0	0.017	0.001	39.83	-13.96 (1)	0.15 (8)	0.43 (2)	0.14 (12)	0.99 (1)	0.37 (1)	0.32 (1)	
3C 033.0	0.060	0.028	41.63	-13.29 (1)	0.31 (1)	3.55 (1)	0.25 (1)	0.63 (1)	0.39 (1)	0.33 (1)	
3C 033.1	0.181	0.633	41.85	-14.11 (1)	0.22 (5)	2.80 (1)	0.25 (1)	0.57 (1)	0.27 (1)	0.21 (1)	-13.26
3C 035.0	0.067	0.141	40.22	-14.81 (1)	$<$ 1.27	0.62 (23)	0.46 (5)	0.77 (2)	0.62 (15)	–	
3C 040.0	0.019	0.041	39.08	-14.79 (11)	0.32 (32)	1.38 (6)	0.24 (28)	2.32 (1)	0.81 (10)	$<$ 0.52	
3C 052.0	0.285	0.232	$<$ 40.64	$<$ -15.76	–	–	–	–	–	–	
3C 061.1	0.184	0.176	42.05	-13.92 (1)	0.25 (4)	2.63 (1)	0.08 (10)	0.31 (1)	0.16 (1)	0.15 (3)	
3C 063.0	0.173	0.027	41.54	-14.38 (5)	0.23 (4)	1.22 (1)	0.23 (3)	0.29 (2)	0.18 (4)	0.13 (5)	
3C 066B	0.022	0.080	40.11	-13.90 (4)	0.22 (7)	0.87 (1)	0.26 (16)	2.45 (1)	0.56 (9)	–	
3C 075N	0.023	0.180	39.58	-14.50 (1)	$<$ 2.20	$<$ 2.20	0.42 (2)	2.48(1)	$<$ 0.69	0.37 (1)	
3C 076.1	0.033	0.138	39.89	-14.50 (2)	$<$ 0.85	$<$ 0.92	$<$ 0.18	1.57 (1)	0.33 (4)	0.54 (1)	
3C 078.0	0.029	0.173	39.73	-14.53 (3)	0.18 (30)	0.48 (16)	0.18 (13)	1.88 (2)	–	–	
3C 079.0	0.256	0.127	42.39	-13.91 (1)	0.29 (3)	2.97 (1)	0.05 (2)	0.32 (1)	0.12 (3)	0.11 (7)	
3C 083.1	0.027	0.164	39.40	-14.83 (14)	$<$ 0.72	$<$ 1.25	–	1.35 (3)	–	–	
3C 084.0	0.018	0.163	41.28	-12.55 (1)	0.42 (1)	2.09 (1)	0.64 (1)	1.12 (1)	0.54 (1)	0.51 (1)	
3C 088.0	0.030	0.126	39.98	-14.33 (1)	0.29 (11)	1.44 (2)	0.50 (3)	2.39 (1)	0.97 (1)	0.79 (3)	
3C 089.0	0.139	0.134	40.28	-15.42 (11)	$<$ 1.86	$<$ 1.69	$<$ 1.26	1.43 (7)	–	–	
3C 093.1	0.243	0.389	42.35	-13.89 (1)	0.28 (4)	2.08 (1)	0.28 (3)	1.36 (1)	0.54 (1)	0.55 (1)	
3C 098.0	0.030	0.229	40.52	-13.79 (1)	0.25 (3)	3.01 (1)	0.15 (3)	0.76 (1)	0.34 (10)	0.23 (7)	
3C 105.0	0.089	0.480	40.89	-14.39 (3)	0.26 (28)	3.59 (1)	0.38 (5)	1.59 (1)	0.55 (4)	0.55 (1)	
3C 111.0	0.049	1.647	42.44^a	-12.28^a (1)	–	1.00^a(1)	0.04^a (10)	–	0.03^a (7)	0.03^a (9)	-11.64
3C 123.0	0.218	0.981	41.96	-14.18 (1)	0.61 (32)	1.09 (18)	0.25 (32)	2.34 (1)	0.48 (1)	0.35 (1)	
3C 129.0	0.022	1.058	39.81	-14.20 (1)	$<$ 0.99	$<$ 1.10	0.61 (1)	1.51 (1)	0.50 (1)	0.50 (20)	
3C 129.1	0.022	1.131	$<$ 39.83	$<$ -14.21	–	–	–	–	–	–	
3C 130.0	0.032	1.309	$<$ 40.17	$<$ -14.19	–	–	–	–	–	–	
3C 132.0	0.201	0.482	41.37	-14.75 (1)	0.90 (5)	1.24 (2)	$<$0.20	1.78 (1)	0.67 (2)	0.73 (2)	
3C 133.0	0.278	0.949	42.41	-13.97 (1)	0.32 (1)	2.26 (1)	0.25 (9)	0.70 (1)	0.17 (1)	0.14 (1)	
3C 135.0	0.125	0.115	41.52	-14.09 (1)	0.33 (3)	3.40 (1)	0.18 (2)	0.80 (1)	0.30 (1)	0.30 (3)	
3C 136.1	0.064	0.762	41.41	-13.57 (1)	0.14 (1)	1.08 (1)	0.05 (1)	0.59 (1)	0.20 (1)	0.20 (3)	
3C 153.0	0.277	0.162	41.60	-14.77 (3)	0.23 (15)	1.07 (3)	0.36 (7)	1.21 (3)	0.54 (8)	0.33 (13)	
3C 165.0	0.296	0.174	41.44	-15.00 (15)	0.44 (15)	1.68 (4)	0.31 (32)	1.14 (27)	0.32 (27)	0.33 (27)	
3C 166.0	0.245	0.211	41.51	-14.75 (3)	0.42 (6)	1.40 (2)	0.38 (7)	0.73 (4)	0.41 (16)	0.34 (24)	
3C 171.0	0.238	0.054	42.45	-13.78 (1)	0.36 (1)	2.73 (1)	0.24 (2)	0.57 (1)	0.38 (6)	0.29 (2)	
3C 173.1	0.292	0.044	41.05	-15.38 (7)	$<$ 0.23	0.63 (12)	0.24 (28)	2.04 (3)	0.24 (29)	0.31 (24)	
3C 180.0	0.220	0.098	41.79	-14.36 (1)	0.25 (4)	3.53 (1)	0.10 (28)	0.69 (1)	0.28 (3)	0.19 (5)	
3C 184.1	0.118	0.032	41.79	-13.77 (3)	0.29 (4)	2.71 (1)	0.08 (7)	0.27 (8)	0.11 (1)	0.09 (3)	-13.99
3C 192.0	0.060	0.054	40.95	-13.97 (1)	0.30 (1)	2.48 (1)	0.11 (3)	0.71 (1)	0.35 (1)	0.26 (1)	

Continued on Next Page

Table A.1 – Continued

Name	Redshift	E(B-V)	L(Hα)	F(Hα)	Hβ	[O III]λ5007	[O I]λ6364	[N II]λ6584	[S II]λ6716	[S II]λ6731	F(Hα) broad
3C 196.1	0.198	0.065	41.56	-14.48 (2)	0.22 (10)	0.91 (3)	0.20 (15)	1.19 (1)	0.52 (1)	0.49 (1)	
3C 197.1	0.128	0.041	40.69	-14.93 (3)	0.37 (11)	1.69 (2)	0.33 (8)	0.76 (4)	0.29 (11)	0.31 (9)	-13.95
3C 198.0	0.082	0.026	41.31	-13.89 (1)	0.27 (1)	0.46 (1)	0.05 (9)	0.28 (1)	–	–	
3C 213.1	0.194	0.028	41.01	-15.02 (3)	0.21 (14)	1.13 (3)	0.46 (6)	1.41 (2)	0.38 (10)	0.28 (12)	
3C 219.0	0.175	0.018	41.55	-14.38 (2)	0.25 (10)	1.67 (1)	0.44 (3)	0.90 (1)	0.24 (6)	0.24 (7)	-13.87
3C 223.0	0.137	0.012	41.68	-14.01 (1)	0.23 (5)	3.09 (1)	0.19 (3)	0.63 (1)	0.25 (3)	0.21 (3)	
3C 223.1	0.107	0.017	41.16	-14.30 (1)	0.28 (7)	2.63 (1)	0.06 (15)	0.81 (1)	0.22 (4)	0.19 (5)	
3C 227.0	0.086	0.026	41.08	-14.17 (2)	0.44 (1)	4.73 (1)	0.22 (13)	0.19 (4)	0.16 (5)	0.16 (11)	-12.52
3C 234.0	0.185	0.019	42.64	-13.33 (1)	0.25 (2)	2.96 (1)	0.04 (8)	0.28 (1)	0.08 (3)	0.07 (1)	-13.29
3C 236.0	0.099	0.011	41.13	-14.25 (1)	0.22 (4)	0.57 (2)	0.30 (3)	0.69 (1)	0.49 (2)	0.35 (3)	
3C 258.0	0.165	0.020	40.96	-14.90 (23)	0.11 (24)	0.17 (15)	< 0.47	< 2.14	–	–	
3C 264.0	0.022	0.023	39.68	-14.35 (1)	0.27 (7)	0.33 (10)	0.22 (9)	1.45 (1)	0.33 (8)	0.33 (22)	
3C 270.0	0.007	0.018	39.26	-13.80 (–)	0.20 (–)	0.51 (–)	0.49 (–)	2.60 (–)	0.72 (–)	0.57 (–)	
3C 272.1	0.004	0.040	38.92	-13.57 (1)	0.10 (3)	0.19 (4)	0.23 (6)	1.28 (1)	0.52 (1)	0.34 (1)	
3C 273.0	0.158	0.021	–	–	–	–	–	–	–	–	-11.51
3C 274.0	0.004	0.022	39.50	-13.11 (1)	0.17 (1)	0.31 (1)	0.36 (1)	2.32 (1)	0.68 (1)	0.77 (1)	
3C 277.3	0.086	0.012	40.83	-14.43 (1)	0.19 (9)	1.29 (1)	0.29 (5)	0.79 (3)	0.32 (1)	0.28 (5)	
3C 284.0	0.239	0.016	41.41	-14.82 (7)	0.20 (12)	1.52 (1)	< 0.24	0.61 (11)	< 0.45	< 0.41	
3C 285.0	0.079	0.017	40.66	-14.52 (1)	0.19 (6)	0.78 (1)	0.10 (10)	0.54 (2)	0.27 (4)	0.19 (6)	
3C 287.1	0.216	0.025	41.50	-14.62 (3)	0.27 (9)	1.71 (1)	0.48 (4)	0.68 (4)	0.29 (7)	0.29 (7)	-13.85
3C 288.0	0.245	0.007	40.86	-15.40 (6)	0.58 (17)	0.62 (16)	0.40 (13)	1.87 (3)	0.85 (7)	0.60 (9)	
3C 293.0	0.045	0.017	40.18	-14.49 (3)	0.19 (17)	0.42 (10)	0.26 (3)	0.88 (1)	0.66 (2)	0.66 (10)	
3C 296.0	0.025	0.025	39.87	-14.28 (1)	0.30 (12)	0.81 (2)	0.22 (23)	1.84 (1)	0.43 (2)	0.38 (10)	
3C 300.0	0.272	0.035	41.78	-14.58 (2)	0.25 (9)	1.71 (1)	0.15 (13)	0.48 (4)	0.33 (4)	0.23 (4)	
3C 303.0	0.141	0.019	41.33	-14.39 (1)	0.35 (4)	2.55 (1)	0.41 (2)	1.06 (1)	0.46 (2)	0.39 (3)	-13.46
3C 303.1	0.269	0.036	42.10	-14.24 (1)	0.26 (2)	2.07 (1)	0.24 (3)	1.03 (1)	0.38 (2)	0.48 (1)	
3C 305.0	0.042	0.026	40.92	-13.68 (1)	0.12 (4)	1.30 (1)	0.17 (7)	1.77 (1)	0.48 (1)	0.40 (1)	
3C 310.0	0.054	0.042	40.32	-14.50 (1)	0.23 (7)	0.54 (3)	0.30 (4)	1.74 (1)	0.84 (1)	0.74 (2)	
3C 314.1	0.120	0.020	40.31	-15.25 (4)	0.37 (16)	0.24 (24)	0.18 (23)	0.53 (7)	0.52 (8)	0.33 (13)	
3C 315.0	0.108	0.062	41.15	-14.32 (1)	0.20 (4)	0.53 (1)	0.25 (2)	0.72 (1)	0.51 (1)	0.37 (2)	
3C 317.0	0.034	0.037	40.35	-14.08 (1)	0.30 (5)	1.00 (2)	0.25 (5)	1.92 (1)	0.58 (1)	0.49 (1)	
3C 318.1	0.044	0.035	39.95	-14.70 (4)	< 0.58	0.26 (32)	0.21 (19)	1.02 (3)	0.29 (9)	0.16 (13)	
3C 319.0	0.189	0.012	41.16	-14.84 (7)	< 0.13	< 0.10	< 0.27	0.30 (6)	0.15 (25)	< 0.14	
3C 321.0	0.097	0.044	40.50	-14.87 (2)	0.30 (11)	2.58 (1)	0.06 (28)	0.50 (3)	0.18 (8)	0.15 (11)	
3C 323.1	0.264	0.042	42.21	-14.12 (1)	0.26 (11)	3.93 (1)	0.13 (20)	0.29 (32)	0.10 (11)	0.08 (21)	-12.37
3C 326.0	0.090	0.053	40.28	-15.02 (5)	< 0.23	1.31 (4)	0.37 (13)	1.93 (3)	0.41 (12)	0.50 (11)	
3C 327.0	0.104	0.089	41.73	-13.70 (1)	0.27 (4)	3.20 (1)	0.14 (1)	0.73 (1)	0.30 (1)	0.24 (1)	
3C 332.0	0.151	0.024	41.31	-14.47 (2)	0.28 (8)	3.14 (1)	0.21 (9)	0.97 (1)	0.37 (6)	0.36 (7)	-12.77
3C 338.0	0.032	0.012	40.25	-14.11 (1)	0.18 (19)	0.21 (6)	0.18 (2)	1.63 (1)	0.41 (1)	0.33 (1)	
3C 346.0	0.163	0.067	41.24^a	-14.62^a (1)	0.20^a (10)	1.00^a (2)	0.14^a (14)	0.84^a (4)	0.13^a (11)	0.13^a (11)	
3C 348.0	0.154	0.094	41.29	-14.51 (1)	0.25 (5)	0.13 (9)	0.27 (5)	1.27 (1)	–	–	
3C 349.0	0.206	0.031	41.50	-14.58 (2)	0.40 (6)	1.54 (2)	0.25 (13)	0.90 (2)	0.34 (5)	0.28 (8)	
3C 353.0	0.030	0.439	40.42	-13.90 (1)	0.20 (17)	0.53 (7)	0.30 (2)	1.09 (1)	0.56 (1)	0.43 (1)	
3C 357.0	0.166	0.045	40.92	-14.96 (3)	0.23 (16)	1.08 (4)	0.46 (7)	1.37 (4)	–	–	

Continued on Next Page

Table A.1 – Continued

Name	Redshift	E(B-V)	L(Hα)	F(Hα)	Hβ	[O III]λ5007	[O I]λ6364	[N II]λ6584	[S II]λ6716	[S II]λ6731	F(Hα) broad
3C 371.0	0.050	0.036	40.94	-13.82 (1)	0.29 (10)	1.01 (4)	0.51 (2)	1.14 (1)	0.32 (3)	0.29 (1)	
3C 379.1	0.256	0.062	41.41	-14.89 (6)	0.31 (6)	2.80 (1)	0.21 (19)	1.54 (5)	0.30 (13)	0.28 (14)	
3C 381.0	0.161	0.053	41.79	-14.05 (1)	0.31 (2)	3.83 (1)	0.11 (9)	0.53 (1)	–	–	
3C 382.0	0.058	0.070	41.39	-13.51 (1)	0.31 (1)	2.45 (1)	0.20 (6)	1.49 (1)	0.12 (8)	0.13 (9)	-11.61
3C 386.0	0.017	0.335	40.17	-13.63 (1)	< 1.08	< 1.08	0.10 (17)	0.57 (1)	0.11 (7)	0.08 (10)	
3C 388.0	0.091	0.080	40.83	-14.47 (2)	0.23 (14)	0.74 (3)	0.26 (13)	2.33 (1)	0.41 (1)	0.37 (1)	
3C 390.3	0.056	0.071	41.57	-13.29 (1)	0.32 (1)	3.24 (1)	0.27 (1)	0.47 (1)	0.10 (1)	0.10 (1)	-11.60
3C 401.0	0.201	0.059	41.01	-15.05 (3)	0.30 (15)	1.10 (5)	0.24 (16)	1.77 (2)	0.46 (9)	0.34 (14)	
3C 402.0	0.024	0.121	39.08	-15.03 (3)	< 1.95	< 2.19	0.37 (13)	2.97 (1)	< 0.44	< 0.97	
3C 403.0	0.059	0.187	41.20	-13.71 (1)	0.25 (3)	3.54 (1)	0.13 (3)	0.84 (1)	0.25 (1)	0.24 (2)	
3C 403.1	0.056	0.234	39.99	-14.87 (15)	0.53 (13)	0.75 (7)	0.29 (17)	0.78 (6)	0.90 (3)	0.72 (11)	
3C 410.0	0.249	0.050	41.86	-14.40 (8)	0.12 (13)	1.46 (1)	0.18 (9)	1.04 (1)	0.37 (3)	0.30 (3)	-13.47 (1)
3C 424.0	0.127	0.096	41.07	-14.55 (1)	0.24 (6)	0.54 (3)	0.27 (5)	0.79 (1)	0.44 (3)	0.40 (12)	
3C 430.0	0.054	0.630	40.12	-14.72 (3)	< 1.09	1.61 (9)	0.33 (20)	1.43 (1)	0.37 (8)	0.40 (4)	
3C 433.0	0.102	0.145	41.40	-14.01 (1)	0.19 (4)	1.88 (1)	0.22 (3)	1.09 (1)	0.46 (2)	0.30 (1)	
3C 436.0	0.214	0.089	41.07	-15.06 (10)	0.20 (22)	3.09 (1)	–	2.08 (9)	0.63 (19)	0.49 (18)	
3C 438.0	0.290	0.358	41.55	-14.87 (1)	< 0.54	< 0.82	< 0.67	1.61 (1)	< 0.66	0.46 (28)	
3C 442.0	0.026	0.065	39.78	-14.40 (1)	0.08 (24)	0.27 (7)	0.19 (8)	1.84 (1)	0.35 (5)	0.45 (1)	
3C 445.0	0.056	0.083	42.50[a]	-12.37[a] (1)	–	1.00[a] (1)	0.04[a] (6)	–	0.02[a] (10)	0.02[a] (10)	-12.03
3C 449.0	0.017	0.167	39.71	-14.09 (1)	0.10 (23)	0.30 (24)	0.13 (9)	1.38 (1)	0.29 (7)	0.22 (1)	
3C 452.0	0.081	0.137	41.16	-14.05 (1)	0.23 (5)	1.53 (1)	0.27 (2)	1.08 (1)	0.36 (1)	0.29 (1)	
3C 456.0	0.233	0.038	42.48	-13.72 (1)	0.32 (1)	2.15 (1)	0.15 (2)	0.78 (1)	0.22 (1)	0.24 (1)	
3C 458.0	0.289	0.082	41.58	-14.84 (4)	<0.45	2.85 (3)	0.33 (14)	0.91 (3)	0.36 (4)	0.31 (8)	
3C 459.0	0.220	0.066	42.13	-14.02 (1)	0.18 (6)	0.82 (1)	0.14 (1)	1.36 (1)	0.45 (1)	0.30 (1)	-13.83
3C 459.0	0.220	0.066	42.17	-13.97 (1)	0.16 (6)	0.73 (1)	0.12 (1)	1.77 (1)	0.35 (1)	0.33 (1)	
3C 460.0	0.269	0.092	42.09	-14.25 (3)	0.25 (3)	0.49 (7)	0.39 (4)	1.23 (2)	0.60 (1)	0.54 (4)	
3C 465.0	0.030	0.069	40.15	-14.17 (1)	0.17 (27)	0.46 (6)	0.26 (9)	2.77 (1)	0.47 (1)	0.32 (1)	

Column description: (1) source name; (2) redshift; (3) Galactic absorption; (4) logarithm of the luminosity of the Hα narrow line, in erg s^{-1}; (5) logarithm of the Hα flux in erg cm^{-2} s^{-1}; (6 through 11) de-reddened flux ratios of the key diagnostic lines with respect to Hα. The values in parentheses report the errors (in percentage) of each line. Missing values marked with '–' correspond to lines outside the coverage of the spectra or severely affected by telluric bands. When no lines are visible we only give the upper limit for Hα; (12) logarithm of the flux of the Hα broad component, when visible.
Notes: (a) for 3C 111, 3C 346, and 3C 445, no narrow Hα measurement is possible and we give instead the [O III] luminosity, referring the flux ratios to this line. No narrow lines are visible in 3C 273 and we only report its broad Hα flux. Data for 3C 270 are taken from Ho et al. (1997) and corrected for Galactic reddening.

Table A.2. Multiwavelength data and spectroscopic classification

Name	redshift	Emission lines		Radio emission		Host magnitude	Classification		
		Hα	[O III]	L_{178}	P_{core}	M_H	FR	spec	Method
3C 015	0.073	40.40	40.60	33.30	31.64	-25.29		LEG	E.I.
3C 017	0.2198	41.88	41.99	34.44	32.94	-24.81*	2	BLO	E.I.
3C 018	0.188	41.93	42.55	34.27	32.00	–	2	BLO	E.I.
3C 020	0.174	41.37	41.54	34.55	30.44	-24.64*	2	HEG	E.I.
3C 028	0.1952	41.51	40.96	34.24	29.33	–		ELEG	E.I.
3C 029	0.0448	40.06	40.09	32.84	30.63	-25.44	1	LEG	E.I.
3C 031	0.0167	39.83	39.46	32.01	29.75	-25.51	1	LEG	E.I.
3C 033	0.0596	41.63	42.18	33.65	30.36	-24.75	2	HEG	E.I.
3C 033.1	0.1809	41.85	42.30	34.07	31.19	-24.47*	2	BLO	E.I.
3C 035	0.0670	40.22	40.01	33.05	30.36	-25.17	2	–	
3C 040	0.0185	39.08	39.22	32.29	30.66	–	1	LEG	E.I.
3C 052	0.2854	<40.64	–	34.53	31.29	-26.74*	2	–	
3C 061.1	0.184	42.05	42.47	34.47	30.49	-23.50*	2	HEG	E.I.
3C 063	0.175	41.54	41.63	34.21	31.12	–		HEG	E.I.
3C 066B	0.0215	40.11	40.05	32.40	30.27	-26.25*	1	LEG	E.I.
3C 075N	0.0232	39.58	<39.92	32.49	29.67	-24.51*	1	–	
3C 076.1	0.0324	39.89	<39.85	32.46	29.37	-24.08*	1	–	
3C 078	0.0286	39.73	39.41	32.51	31.25	-26.16	1	LEG	D.D.
3C 079	0.2559	42.39	42.86	34.78	31.39	-25.27	2	HEG	E.I.
3C 083.1	0.0255	39.40	<39.50	32.57	29.48	-26.70*	1	–	
3C 084	0.0176	41.28	41.60	32.62	32.46	-25.99		LEG	E.I.
3C 088	0.0302	39.98	40.14	32.49	30.57	-24.81	2	LEG	E.I.
3C 089	0.1386	40.28	<40.51	34.01	31.39	-26.22	1	–	
3C 093.1	0.2430	42.35	42.67	34.24	–	–		HEG	E.I.
3C 098	0.0304	40.52	41.00	32.99	29.87	-24.38	2	HEG	E.I.
3C 105	0.089	40.89	41.45	33.54	30.46	-24.31	2	HEG	E.I.
3C 111	0.0485	–	42.44	33.54	31.77	-25.07	2	BLO	O.R.
3C 123	0.2177	41.96	42.00	35.41	32.00	-26.58*		LEG	E.I.
3C 129	0.0208	39.81	<39.85	32.65	29.51	-25.11	1	–	
3C 129.1	0.0222	<39.83	–	32.06	28.53	-25.61	1	–	
3C 130	0.1090	<40.17	–	33.66	30.94	-28.45	1	–	
3C 132	0.214	41.37	41.46	34.25	31.58	-26.00	2	LEG	D.D.
3C 133	0.2775	42.41	42.76	34.72	32.53	-25.36*	2	HEG	E.I.
3C 135	0.1253	41.52	42.05	33.84	30.31	-24.47	2	HEG	E.I.
3C 136.1	0.064	41.41	41.44	33.13	29.16	-25.17	2	HEG	E.I.
3C 153	0.2769	41.60	41.63	34.56	29.94	-25.60*	2	LEG	E.I.
3C 165	0.2957	41.44	41.67	34.57	31.30	-25.80*	2	LEG	E.I.
3C 166	0.2449	41.51	41.66	34.42	32.92	-25.32*	2	LEG	E.I.
3C 171	0.2384	42.45	42.89	34.51	30.55	-24.73*	2	HEG	E.I.
3C 173.1	0.2921	41.05	40.85	34.61	31.39	-26.48	2	LEG	O.R.
3C 180	0.22	41.79	42.34	34.32	–	-24.94	2	HEG	E.I.
3C 184.1	0.1182	41.79	42.23	33.66	30.37	-24.22*	2	BLO	E.I.
3C 192	0.0598	40.95	41.34	33.25	29.82	-24.68	2	HEG	E.I.
3C 196.1	0.198	41.56	41.52	34.31	31.82	-25.47	2	LEG	E.I.
3C 197.1	0.1301	40.69	40.92	33.55	30.43	-24.94	2	BLO	E.I.
3C 198	0.0815	41.31	40.97	33.19	–	-23.62*		SF	D.D.
3C 213.1	0.194	41.01	41.06	33.84	31.15	-25.02*	2	LEG	E.I.
3C 219	0.1744	41.55	41.77	34.53	31.69	-25.70	2	BLO	E.I.
3C 223	0.1368	41.68	42.17	33.85	30.70	-24.74	2	HEG	E.I.
3C 223.1	0.107	41.16	41.58	33.23	30.36	-24.95	2	HEG	E.I.
3C 227	0.0861	41.08	41.75	33.74	30.58	-24.90	2	BLO	E.I.
3C 234	0.1848	42.64	43.11	34.47	32.04	-26.09	2	HEG	E.I.
3C 236	0.1005	41.13	40.89	33.56	31.62	-25.34	2	LEG	E.I.
3C 258	0.165	40.96	40.19	33.85	–	–		–	
3C 264	0.0217	39.68	39.20	32.43	30.32	-25.09	1	LEG	E.I.
3C 270	0.007	39.26	38.96	31.79	29.57	-25.01	1	LEG	E.I.
3C 272.1	0.0035	38.92	38.20	30.72	28.68	-24.43	1	LEG	E.I.
3C 273	0.1583	–	–	34.62	33.65	–		BLO	
3C 274	0.0044	39.50	38.99	32.63	30.21	-25.28	1	LEG	E.I.

Continued on Next Page

Table A.2. Continued

Name	redshift	Emission lines		Radio emission		Host magnitude	Classification		
		Hα	[O III]	L_{178}	P_{core}	M_H	FR	Class	Method
3C 277.3	0.0857	40.83	40.94	33.21	30.34	-24.87	2	HEG	E.I.
3C 284	0.2394	41.41	41.59	34.28	30.44	-25.57	2	HEG	D.D.
3C 285	0.0794	40.66	40.55	33.23	30.03	-24.53	2	HEG	E.I.
3C 287.1	0.2159	41.50	41.73	34.04	32.71	-25.72	2	BLO	E.I.
3C 288	0.246	40.86	40.65	34.53	31.73	-26.10*	2	LEG	E.I.
3C 293	0.0450	40.18	39.80	32.77	30.67	-25.33		LEG	E.I.
3C 296	0.0240	39.87	39.78	32.22	29.99	-26.04	1	LEG	E.I.
3C 300	0.27	41.78	42.01	34.60	31.27	-24.92	2	HEG	E.I.
3C 303	0.141	41.33	41.74	33.77	31.94	-25.35	2	BLO	E.I.
3C 303.1	0.267	42.10	42.42	34.25	31.04	–	2	HEG	E.I.
3C 305	0.0416	40.92	41.03	32.79	30.07	-25.26	2	HEG	E.I.
3C 310	0.0535	40.32	40.05	33.56	30.72	-25.02*	2	LEG	E.I.
3C 314.1	0.1197	40.31	39.69	33.59	29.56	–		ELEG	E.I.
3C 315	0.1083	41.15	40.87	33.72	31.64	-24.74*		LEG	E.I.
3C 317	0.0345	40.35	40.35	33.12	31.02	-26.04		LEG	E.I.
3C 318.1	0.0453	39.95	39.36	32.72	29.12	-25.70		–	
3C 319	0.192	41.16	<40.16	34.20	31.49	-24.41*	2	–	
3C 321	0.096	40.50	40.91	33.49	30.89	-25.52	2	HEG	E.I.
3C 323.1	0.264	42.21	42.80	34.31	31.89	-26.74	2	BLO	E.I.
3C 326	0.0895	40.28	40.40	33.60	30.45	-24.33	2	LEG	O.R.
3C 327	0.1041	41.73	42.24	33.98	30.99	–	2	HEG	E.I.
3C 332	0.1517	41.31	41.81	33.77	30.79	-25.38	2	BLO	E.I.
3C 338	0.0303	40.25	39.57	32.99	30.34	-26.21*	1	LEG	E.I.
3C 346	0.161	–	41.24	33.88	32.18	-25.84	2	–	
3C 348	0.154	41.29	40.40	35.35	30.80	–		ELEG	D.D.
3C 349	0.205	41.50	41.69	34.20	31.35	-24.82*	2	LEG	E.I.
3C 353	0.0304	40.42	40.14	33.69	30.61	-24.77	2	LEG	E.I.
3C 357	0.1662	40.92	40.95	33.86	30.63	-25.83*	2	LEG	D.D.
3C 371	0.0500	40.94	40.94	32.33	31.85	-25.36		LEG	E.I.
3C 379.1	0.256	41.41	41.86	34.16	30.90	-25.69	2	HEG	E.I.
3C 381	0.1605	41.79	42.37	34.06	30.63	-24.81	2	HEG	D.D.
3C 382	0.0578	41.39	41.78	33.19	31.22	-26.03	2	BLO	E.I.
3C 386	0.0170	40.17	<40.20	32.18	28.95	-24.57		–	
3C 388	0.091	40.83	40.70	33.70	31.15	-26.20	2	LEG	E.I.
3C 390.3	0.0561	41.57	42.08	33.54	31.46	-24.84	2	BLO	E.I.
3C 401	0.2010	41.01	41.05	34.38	31.67	-25.03*	2	LEG	E.I.
3C 402	0.0239	39.08	<39.42	32.11	29.79	-24.77*	1	–	
3C 403	0.0590	41.20	41.75	33.16	29.96	-25.27	2	HEG	E.I.
3C 403.1	0.055	39.99	39.86	32.98	–	-24.36		LEG	E.I.
3C 410	0.248	41.86	42.02	34.80	33.43	–	2	BLO	E.I.
3C 424	0.127	41.07	40.80	33.78	30.87	-23.96*		LEG	E.I.
3C 430	0.0541	40.12	40.33	33.36	30.06	-25.28	2	LEG	O.R.
3C 433	0.1016	41.40	41.67	34.16	30.11	-25.79*		HEG	E.I.
3C 436	0.2145	41.07	41.56	34.37	31.39	-25.50	2	HEG	D.D.
3C 438	0.290	41.55	<41.46	35.07	31.65	-26.57	1	–	
3C 442	0.0263	39.78	39.21	32.39	28.49	–		LEG	E.I.
3C 445	0.0562	–	42.50	33.26	31.42	–	2	BLO	O.R.
3C 449	0.0171	39.71	39.19	31.87	29.38	-24.80*	1	LEG	E.I.
3C 452	0.0811	41.16	41.34	33.94	31.34	-24.92	2	HEG	E.I.
3C 456	0.2330	42.48	42.81	34.23	31.57	–	2	HEG	E.I.
3C 458	0.289	41.58	42.03	34.58	30.88	–	2	HEG	E.I.
3C 459	0.2199	42.17	42.03	34.55	33.20	-25.34*	2	BLO	E.I.
3C 460	0.268	42.09	41.78	34.25	31.52	–	2	LEG	E.I.
3C 465	0.0303	40.15	39.81	32.89	30.74	-26.44*	1	LEG	E.I.

Column description: (1) 3CR name; (2) redshift from Spinrad et al. (1985); (3) and (4) logarithm of Hα and [O III]λ5007 luminosities [erg s^{-1}] from Buttiglione et al. (2009); (5) radio luminosity at 178 MHz [erg s^{-1} Hz^{-1}] from Spinrad et al. (1985); (6) radio core power at 5 GHz [erg s^{-1} Hz^{-1}] from Baldi & Capetti (2009); (7) host H magnitude from 2MASS (Skrutskie et al. 2006) (or from HST (Donzelli et al. 2007) for the objects marked with a *); (8): morphological FR type; (9) spectroscopic classification into High Excitation Galaxy (HEG); Low Excitation Galaxy (LEG); Broad Line Object (BLO); Extremely Low Excitation Galaxy (ELEG); (SF) starforming galaxy; (–) unclassified. Column (10) classification method: E.I. - excitation index; D.D. - diagnostic diagrams; O.R. - emission line radio correlation.